NASA Technical Memorandum 100967

Fracture Resistance of a TiB_2 Particle/SiC Matrix Composite at Elevated Temperature

Michael G. Jenkins
University of Tokyo
Tokyo, Japan

and

Jonathan A. Salem
Lewis Research Center
Cleveland, Ohio

and

Srinivasa G. Seshadri
Standard Oil Engineered Materials Company
Niagara Falls, New York

June 1988

NASA

FRACTURE RESISTANCE OF A TiB_2 PARTICLE/SiC MATRIX COMPOSITE AT ELEVATED TEMPERATURE

Michael G. Jenkins*
Institute of Industrial Science
University of Tokyo
Tokyo, Japan

Jonathan A. Salem
National Aeronautics and Space Administration
Lewis Research Center
Cleveland, Ohio 44135

and

Srinivasa G. Seshadri
Standard Oil Engineered Materials Company
P.O. Box 1054
Niagara Falls, New York 14302

SUMMARY

The fracture resistance of a commercial TiB_2 particle/SiC matrix composite was evaluated at temperatures ranging from 20 to 1400 °C. A laser interferometric strain gauge (LISG) was used to continuously monitor the crack mouth opening displacement (CMOD) of the chevron-notched and straight-notched, three-point bend specimens used. Crack growth resistance curves (R-curves) were determined from the load versus displacement curves and displacement calibrations. Fracture toughness, work-of-fracture, and R-curve levels were found to decrease with increasing temperature. Microstructure, fracture surface, and oxidation coat were examined to explain the fracture behavior.

E-3842-1

INTRODUCTION

Elevated temperature applications, such as components of advanced heat engines (refs. 1 to 3), require advanced ceramic materials because of their high-temperature strengths, resistances to thermal shock, low densities, low thermal conductivities, and corrosion resistances. They are traditionally considered to be brittle materials at room temperature; however, at elevated temperatures, various mechanical properties may be expected to change (e.g., K_{IC} or R-curves may vary with temperature). Since the required applications of ceramics are at elevated temperature, the fracture resistance of these materials must be determined as a function of temperature.

A commercial 16 vol % TiB_2 particle/SiC matrix composite[1] was investigated for its fracture resistance at elevated temperatures. It is a ceramic material

---

*Currently an invited researcher at NASA Lewis Research Center.

[1]Hexoloy ST, Standard Oil Engineered Materials Company, Niagara Falls, New York.

that can be easily machined using electric discharge methods (refs. 4 and 5). Figures 1(a) and (b) show its microstructure in the as-received state and after exposure in air to 1400 °C. Some typical properties are summarized in table I. Previous studies of this composite material (refs. 6 and 7) have shown that the mechanical properties and the fracture toughness have some dependence on temperature from 20 to 1400 °C. However, previous unavailability of this composite material has precluded more extensive investigations of the crack growth resistance as a function of temperature.

This paper reports the results of a study of the fracture resistance of a TiB_2 particle/SiC matrix composite in the temperature range of 20 to 1400 °C using chevron-notched and straight-notched three-point bend specimens. A recently developed procedure using a laser interferometric strain gauge (LISG) was used to monitor specimen crack mouth opening displacements (CMOD). Such displacements are not affected by the loading system compliance which may vary with temperature (refs. 8 and 9). These results show that the fracture toughness, work-of-fracture, and crack growth resistance definitely depend on temperature over the range of 20 to 1400 °C, with this temperature dependence being related to thermally activated mechanisms in the microstructure.

TEST SPECIMENS AND PROCEDURES

Specimens

Three chevron-notched and three straight-notched, three-point bend specimens were tested from 20 to 1400 °C in 200 °C increments. All specimens were 6.36 by 6.36 by 50 mm with a loading span of 40 mm. Figure 2 shows the specimen types and symbols.

The initial notch depth ratios, $\alpha_o = a_o/W$, were 0.44 and 0.50 for the chevron-notches and the straight-notches, respectively. The notches were machined with a rotating, diamond-tipped saw blade which produced a notch width of 0.300 mm.

Procedure

All testing was performed in ambient air with a screw-type load frame[2] under displacement control. The upper push rod and lower support fixture were fabricated from sintered alpha silicon carbide. A cross head speed of 0.01 mm/min was maintained continuously during all tests. Tests were performed in a refractory brick furnace using silicon carbide resistance-bar heating elements. Transparent fused silica view ports in the furnace wall allowed the passage of the LISG laser beams.

Application of the LISG to the fracture testing of ceramics has been previously reported by Jenkins et al. (ref. 9); however, it is reviewed here for clarity. Interference fringes are created by the reflection of an incident laser beam from diffraction targets located at the mouth of the specimen notch. As the CMOD increases, the fringe patterns move relative to the recording device. The passage of each whole-order fringe is equal to approximately

---

[2]Instron Corporation, Canton, Massachusetts. Model TTDML.

1.0 mm of crack mouth opening displacement within a resolution of 0.25 mm. The fringe motion and the applied test load are simultaneously recorded during the fracture testing to produce the plots of load versus CMOD.

TEST RESULTS AND DISCUSSION

Fracture Toughness

Test results are presented as a function of test temperature in table II. The straight-notched test specimens did not exhibit stable crack growth at any test temperature. However, sustained stable crack growth was consistently observed for the chevron-notched specimens. This latter stable crack growth occasionally followed a small, unstable crack initiation. Figure 3 illustrates representative load versus CMOD test records for both specimen types.

Apparent fracture toughness values for the chevron-notched specimens were calculated from the maximum load and minimum stress intensity factor coefficient as proposed by Pook (ref. 10) and verified by Munz et al. (ref. 11), such that:

$$K_{IC} = Y^*_{min} P_{max} / (B\, W^{1/2}) \qquad (1)$$

where K_{IC} is the fracture toughness, Y^*_{min} is the minimum stress intensity factor coefficient, P_{max} is the maximum load, B is the specimen thickness, and W is the specimen width. Relationships have been reported by Jenkins et al. (ref. 12) for the stress intensity factor coefficient, Y*, for the chevron-notched, three-point bend specimen. Apparent fracture toughness values for the straight-notched specimens were calculated from the maximum load and the relationships of Tada et al. (ref. 13) for the stress intensity factor coefficient.

The apparent fracture toughnesses obtained are shown in figure 4. The values from the chevron-notched specimens are lower than those of the straight-notched specimens because geometry of the chevron-notch prevents overloading and provides stable crack extension. Overloading is prevented by the stress concentration at the chevron tip, while the stability is due to the simultaneous increase in compliance and crack front length with crack extension for chevron-notch geometry. As a result of this stable growth (ref. 12), reliable work-of-fracture values and crack growth resistance curves can be obtained using the chevron-notched specimen.

The apparent fracture toughness determined from the chevron-notched specimen better represents fracture behavior of a sharp crack than the relatively blunt notch tip of the straight-notched specimen. The scatter bands of the straight-notched specimen fracture toughness data indicate the difficulties of obtaining consistent and controlled crack initiation in this material.

The fracture toughness results of this study and those of previous studies of similar TiB_2 particle/SiC matrix composites are compared in table III. The insensitivity of the straight-notched specimens to temperature can be explained in terms of the effects of temperature on strength. The strength of this composite is nearly independent of temperature to 1200 °C (ref. 7). A specimen with a blunt, straight notch measures the notch strength of the material. Such

a measurement is between the extreme cases of an unnotched strength specimen and a specimen with a sharp crack. The use of blunt notches has been noted to overestimate fracture toughness (refs. 14 and 15).

Work Fracture

The work-of-fracture is calculated by dividing the area under the load versus load point displacement curve by the fracture surface area, which is twice the total projected area of one fracture face. A schematic of the calculation of the work-of-fracture, after Nakayama (ref. 16) and Tattersall and Tappin (ref. 17), is shown in figure 5.

Relationships between the CMOD and the load point displacement (LPD) from Jenkins et al. (ref. 12) and Tada et al. (ref. 13) were used to determine the load versus LPD curves for the work-of-fracture calculations.

Although calculations from the straight-notched test specimens may not be a useful quantity, since stable crack growth behavior is required for the reliable calculation of the work-of-fracture (ref. 18), the values are presented for comparison. The work-of-fracture values are plotted versus temperature in figure 6.

Crack Growth Resistance

The R-curves were developed from the stable crack growth regions of the load versus CMOD plots of the chevron-notched specimens and CMOD compliance versus crack length relations (ref. 12). Figure 7 shows a schematic of the calculation of the effective crack length during stable crack growth using the compliance technique. The unloading slopes were assumed to return to zero displacement and load.

The effective crack lengths and the load history were used to calculate the change in the total strain energy for an incremental crack extension such that:

$$G = \Delta U / \Delta A \qquad (2)$$

where G is the strain energy release rate, ΔU is the change in the total strain energy, and ΔA is the incremental change in the fractured area. This procedure is shown schematically in figure 8. The final G_R-curve for each temperature is shown in figure 9. These curves were produced from linear least square fits of the three individual R-curves determined at each temperature. The toughening mechanisms due to the TiB_2 particles in the alpha SiC matrix apparently become less effective at elevated temperatures, since the 1200 and 1400 °C R-curves fall in the same range as R-curves for a monolithic sintered alpha SiC[3] (ref. 19).

---

[3]Hexoloy SA, Standard Oil Engineered Materials Company, Niagara Falls, New York.

MATERIAL ANALYSIS

Microstructrual Characterization

This TiB_2 particle/SiC matrix composite consists of discrete TiB_2 particles in a matrix of equiaxed and elongated SiC grains of 3 μm average size. The as-polished and the etched microstructures of this material in the as-received condition and after testing at 1400 °C are shown in figures 1 and 10. The Murikami's etchant attacks exposed TiB_2 particles leaving the dark spots shown in the micrographs. The high temperature exposure of about 1 hr required for the fracture tests has not visibly altered the microstructure. The micrographs also show evidence that TiB_2 particles pin SiC grain boundaries during sintering.

This material has been reported (ref. 7) to contain 16 vol % particulate loading with sintered compacts achieving 98 to 99 percent of theoretical density. Transmission electron microscopy studies have shown neither extensive chemical reactions or solid solutions at the TiB_2/SiC interface (Private communication from A. Zangvil, University of Illinois, Urbanana, Illinois.). The TiB_2 particles are weakly bonded to the SiC matrix.

Fractography

Figure 11 contrasts room and 1400 °C fracture topographies. The room temperature fracture surfaces consist of ridges and valleys, while the high-temperature fracture surfaces are relatively flat and show signs of deformation. The fracture ridges, evident with the secondary electron mode, are frequently associated groups of TiB_2 particles and pores that are readily visible in the backscattered electron mode, as illustrated in figure 12. It is apparent that the room temperature crack extension occurs by the linking of groups of TiB_2 particles, and that a deviation of the crack path results. This interaction may be the result of TiB_2 particle groups perturbing the applied stress field and attracting the macrocrack tip. As the temperature is increased the effect is relieved and the particles have less influence. The temperature dependence of this crack extension mechanism is seen by comparing the rough fracture surfaces of the room temperature tests (fig. 11(a)) with the smooth fracture surfaces of the 1400 °C test (fig. 11(b)).

The increased toughness of this material has previously been attributed to crack deflection and the compressive component of residual stress associated with the particle/matrix interface (ref. 6). It should be noted, however, that similar isostatic components of tensile residual stress exist ($\sigma_r = \sigma_t = 260$ MPa, refs. 20 and 21) within the particle. Outside the particle/matrix interface, radial (tensile) and tangential (compressive) stresses exist. The significance of these tensile components of stress is supported by figures 13(a) to (c) which show cracking of the particles and the surrounding matrix at low temperatures, and the deformational separation of the particles from the matrix at high-temperatures. The particle separation is not readily visible using the secondary electron mode, however, the backscattered electron mode clearly delineate the particles and cracks. On the basis of this fractography, a plausible explanation for crack path deviations and increased toughness of the material is the development of microcracks at the particle/matrix interface. Groups of microcracked interfaces would attract the macrocrack tip and cause formation of the ridges (crack path deviations). Further,

the microcracks would also redistribute the stresses around the macrocrack tip at low temperatures but would fail to do so at high-temperatures because the residual stresses, which should enhance microcracking, are relieved. The ineffectiveness of the particles to influence the crack path at high-temperature is evidenced by the smooth fracture topography of figure 11(b).

Oxidation

The maximum exposure time of the test samples to the elevated temperatures was approximately 1 hr. To the unaided eye the surface oxidation is a fine white coating on the 800 and 1000 °C test samples, and a rough greenish-white coating on the 1400 °C test samples. At higher magnifications the oxidation product appears as bubbles of glass which contain a white polycrystalline phase. The oxidation coat varies from a layer of 5 to 10 μm particles at 800 °C, to a nearly continuous 25 μm layer at 1400 °C. Beneath the oxide layer of specimens tested at 1400 °C, the material was attacked to a depth of 25 μm. Interconnected porosity extended into the specimens, as shown in figure 14. x-ray analysis of the oxide surface layer showed diffraction peaks corresponding to rutile, TiO_2, along with a single broad band indicative of glassy SiO_2.

CONCLUSIONS

The fracture resistance of this TiB_2 particle/SiC matrix composite shows temperature dependence to 1400 °C. Flat R-curves exist at all temperatures, indicating a constant resistance to fracture. The second phase additives increase the R-curve level by forming microcracks which influence the crack path through the material. However, the particles do not impart increasing crack growth resistance to monolithic SiC. The effect of second phase additions on crack trajectory and R-curve level is reduced with temperature.

Chevron-notched specimens produce sharp, real cracks and provide the means for studying controlled, stable crack growth behavior in nominally brittle materials. The present test technique, using chevron-notch specimens and the laser interferometric strain gauge, illustrates the effects of temperature and second phase constituents (e.g., TiB_2) on R-curve behavior.

REFERENCES

1. Shih, T.T., and Opoku, J., Eng. Fract. Mech., 12, 479 (1979).

2. Katz, P.N., Nitrogen Ceramics, F.L. Riley, ed., p. 643, Nordoff, Leyden, 1977.

3. Godfrey, D.J., Proc. Br. Ceram. Soc., 22, 1 (1973).

4. Garnier, J.E., Boecker, W.D.G., McMurty, C.H., and Calandra, S., "Electric-Discharge Machining of Silicon Carbide Based Materials," presented at the 89th Annual Meeting to the American Ceramic Society, Pittsburgh PA, Paper No. 150-C-87, Apr. 26-30, 1987.

5. Seshadri, S.G., Garnier, J.E., and Chia, K.Y., "Effect of Machining Techniques on the Mechanical Properties of SiC/TiB_2 Composites," presented at the 89th Annual Meeting to the American Ceramic Society, Pittsburgh, PA, Paper No. 149-C-87, Apr. 26-30, 1987.

6. Janney, M.A., Am. Ceram. Soc. Bull., 66, 322 (1987).

7. McMurty, C.H., Boecker, W.D.G., Seshadri , S.G., Zanghi, J.S., and Garnier, J.E., Am. Ceram. Soc. Bull., 66, 325 (1987).

8. Sharpe, W.N., Jr., Handbook on Experimental Mechanics, A.S. Kobayashi, ed., Chapter 13, Prentice Hall, Englewood Cliffs, 1966.

9. Jenkins, M.G., Kobayashi, A.S., Sakai, M., White, K.W., Bradt, R.C., Am. Ceram. Soc. Bull., 66, 1734 (1987).

10. Pook, L.P., Int. J. Fract., 8, 103 (1972).

11. Munz, D.G., Shannon, J.L., Jr., and Bubsey, R.T., Int. J. Fract., 16, R137 (1980).

12. Jenkins, M.G., Kobayashi, A.S., White, K.W., and Bradt, R.C., Int. J. Fract., 34, 281 (1987).

13. Tada, H., Paris, P.C., and Irwin, G.R., The Stress Analysis of Cracks Handbook, Del Research Corporation, Hellerton, PA, 1973.

14. Pabst, R.F., Fracture Mechanics of Ceramics, Vol. 2, R.C. Bradt, D.P.H. Hasselman, and F.F. Lange, eds., p. 555, Plenum Press, New York, 1974.

15. Munz, D., Bubsey, R.T., and Shannon, J.L., Jr., J. Am. Ceram. Soc., 65, 300 (1980).

16. Nakayama, J., Jpn. J. Appl. Phys., 3, 422 (1964).

17. Tattersall, H.G., and Tappin, G., J. Mater. Sci., 1, 296 (1966).

18. Nakayama, J., Abe, H., and Bradt, R.C., J. Am. Ceram. Soc., 64, 671 (1981).

19. Jenkins, M.G., "Ceramic Crack Growth Resistance Determination Utilizing Laser Interferometry," PhD. Dissertation, University of Washington, Seattle, WA, 1987.

20. Selsing, J., J. Am. Ceram. Soc., 44, 419 (1961).

21. Lange, F.F., Fracture Mechanics of Ceramics, Vol. 2, R.C. Bradt, D.P.H. Hasselman, and F.F. Lange, eds., p. 599, Plenum Press, New York, 1974.

22. Chia, K.Y., and Seshadri, S.G., "Sharp Crack Fracture Toughness Testing of Ceramics," presented at the 89th annual meeting of the American Ceramic Society, Pittsburgh, PA, Paper No. 162-C-87, Apr. 26-30, 1987.

Table I. - TYPICAL PROPERITIES OF TiB_2 PARTICLE/SiC MATRIX COMPOSITE

[The technical data are values reported by the producer.]

Producer	Standard Oil Engineered Materials Co. Niagara Falls, New York
Tradename	Hexoloy ST
Oescription	Two phase, sintered 16 vol % TiB_2 particles in a matrix of alpha SiC
Density, kg/m	3300
Modulus of elasticity, GPa at room temperature	427
Poisson's ratio	0.15
Coefficient of thermal expansion, mm/mm °C from room temperature to 700 °C	4.20×10^{-6}

TABLE II. - SUMMARY OF FRACTURE PARAMETER RESULTS

[SN = straight-notch bend bar; CN = chevron-notched bend bar.]

Temperature, °C	Average[a] K_{IC}, MPa $m^{1/2}$	Average[a] work-of-fracture, J/m^2
20 SN	4.63±0.23	25.3±2.38
CN	4.07±0.17	19.2±1.49
200 SN	4.21±0.14	25.2±9.10
CN	3.47±0.04	16.2±0.79
400 SN	4.49±0.26	21.8±5.52
CN	3.59±0.11	16.9±2.27
600 SN	4.73±0.22	23.5±0.57
CN	3.14±0.09	10.1±3.02
800 SN	4.26±0.19	23.3±2.50
CN	3.15±0.18	9.75±1.42
1000 SN	4.32±0.35	20.0±1.10
CN	2.75±0.39	9.86±3.76
1200 SN	4.63±0.64	21.73±4.28
CN	2.81±0.11	7.26±0.07
1400 SN	4.13±0.35	22.9±10.2
CN	2.86±0.27	8.46±1.56

[a]Average ± standard deviation.

Table III. - COMPARISON OF FRACTURE TOUGHNESS MEASUREMENTS OF TiB_2 PARTICLE/SiC MATRIX COMPOSITES

[SNBB = straight-notched bend bar; CNBB = chevron-notched bend bar; IM = indentation method; SCT = sharp crack technique.]

Source	Method	Fracture toughness, MPa $m^{1/2}$							
		Temperature, °C							
		20	200	400	600	800	1000	1200	1400
This study	SNBB	4.6	4.2	4.5	4.7	4.3	4.3	4.6	4.1
	CNBB	4.1	3.5	3.6	3.1	3.2	2.8	2.8	2.9
McMurtry et al. (ref. 7)	SNBB[a]	8.9	---	---	---	---	---	---	---
			---	---	---	---	---	---	---
Janney (ref. 6)	IM[b]	4.5	---	---	---	---	---	---	---
			---	---	---	---	---	---	---
Chia and Seshadri (ref. 22)	SCT	4.0	---	---	---	---	---	---	---
			---	---	---	---	---	---	---

[a]0.9 mm diamond cut notch.
[b]Hot pressed SiC-15 vol % TiB_2 composite.

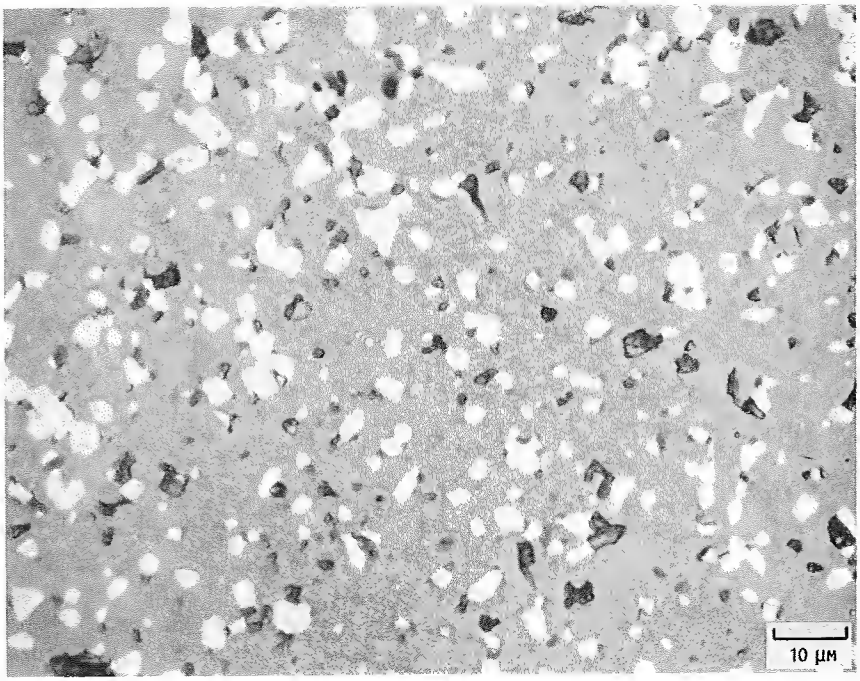

(A) AS-RECEIVED STATE.

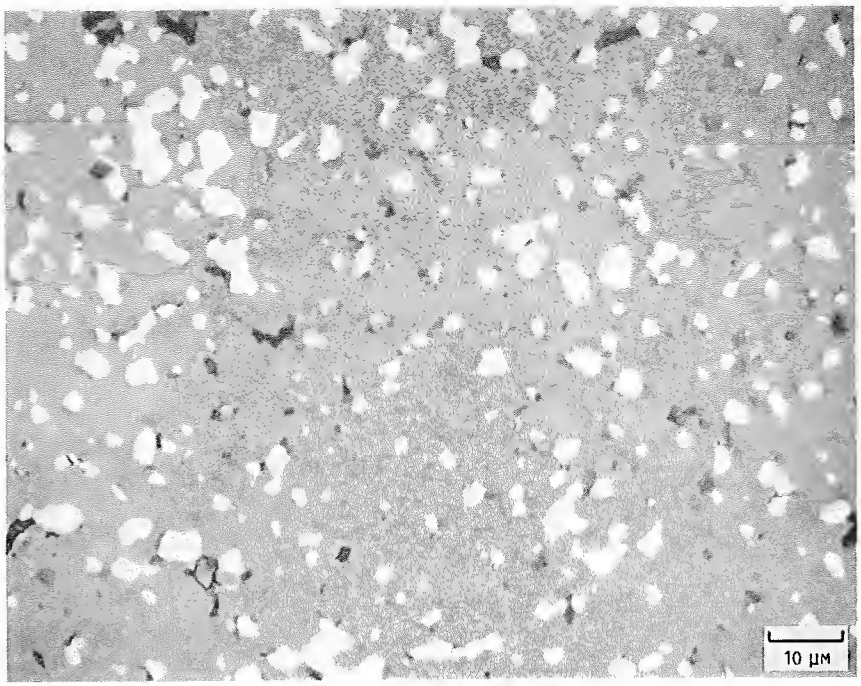

(B) AFTER TESTING AT 1400 ^{0}C. WHITE REGIONS ARE TiB_2 ARTICLES. (1000X).

FIGURE 1. - UNETCHED MICROSTRUCTURE OF TiB_2/SiC COMPOSITE.

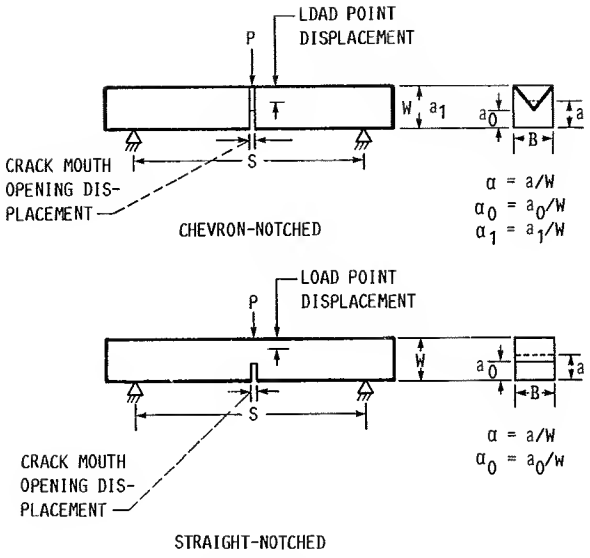

FIGURE 2. - GEOMETRY DF CHEVRON-NDTCHED AND STRAIGHT-NOTCHED SPECIMENS USED IN THIS INVESTIGATION.

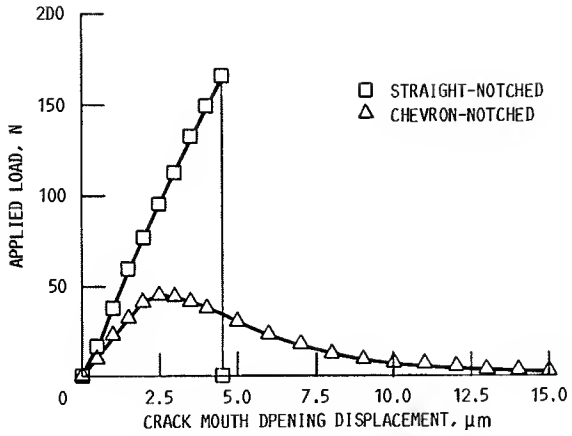

FIGURE 3. - TYPICAL LDAD VERSUS CMOD HISTORIES FOR 20 ^{o}C THREE-PDINT BEND TESTS.

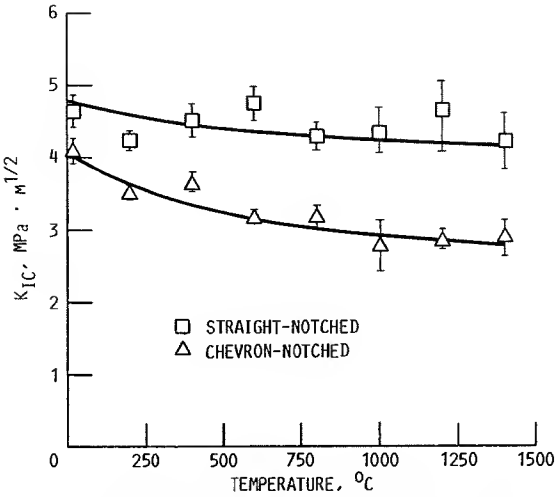

FIGURE 4. - FRACTURE TDUGHNESS AS A FUNCTION OF TEMPERATURE FOR TiB_2/SiC COMPOSITE.

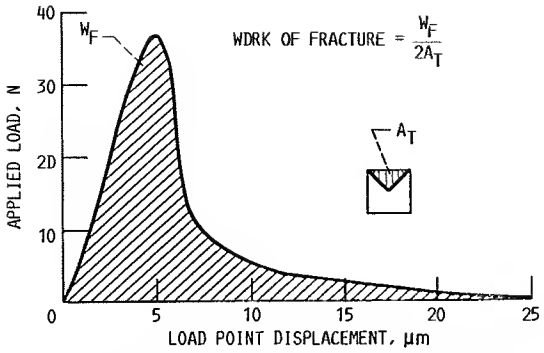

FIGURE 5. - SCHEMATIC DIAGRAM SHOWING CALCULATIDN OF THE WORK-OF-FRACTURE FOR A CHEVRON-NOTCHED SPECIMEN.

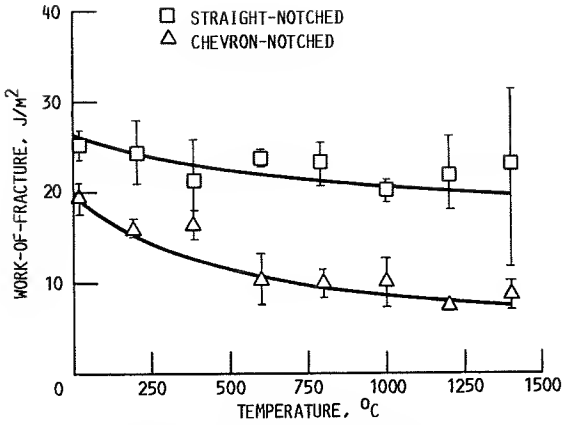

FIGURE 6. - WORK-OF-FRACTURE AS A FUNCTION OF TEMPERATURE FOR TiB_2/SiC COMPOSITE.

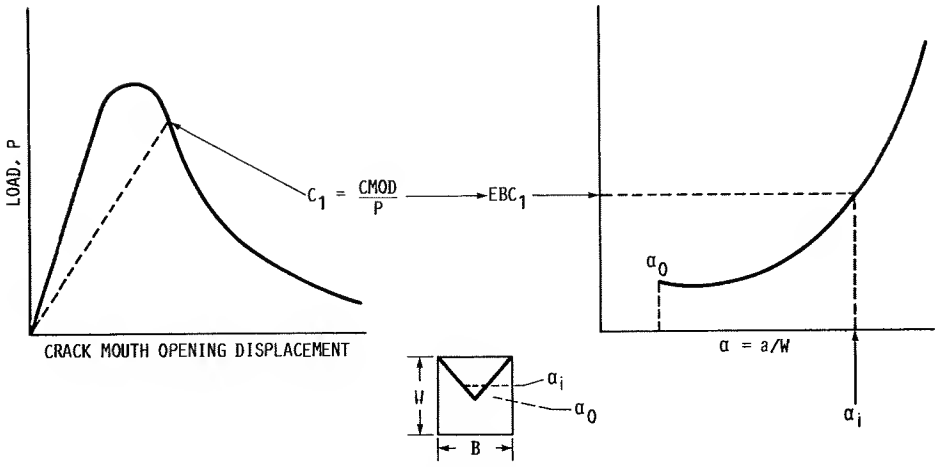

FIGURE 7. - SCHEMATIC DIAGRAM OF CALCULATION OF EFFECTIVE INSTANTANEOUS CRACK LENGTH USING THE COMPLIANCE TECHNIQUE.

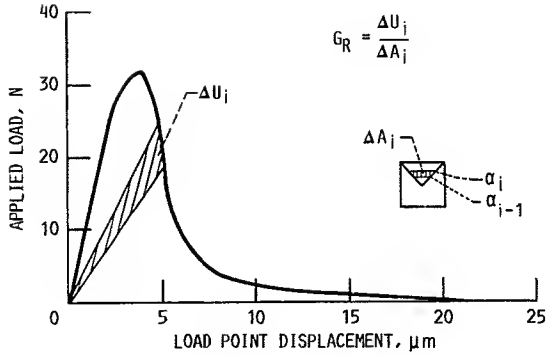

FIGURE 8. - SCHEMATIC DIAGRAM ILLUSTRATING CALCULATION OF G R-CURVE FOR CHEVRON-NOTCHED SPECIMEN.

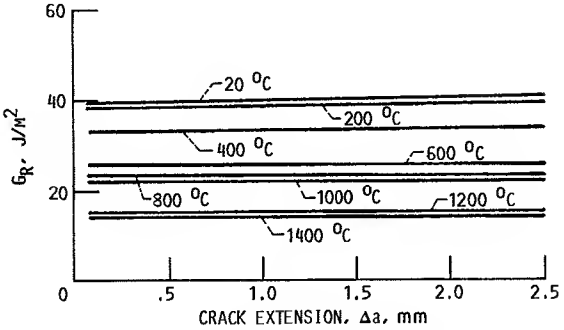

FIGURE 9. - G R-CURVES FOR TiB_2/SiC TESTED AT VARIOUS TEMPERATURES.

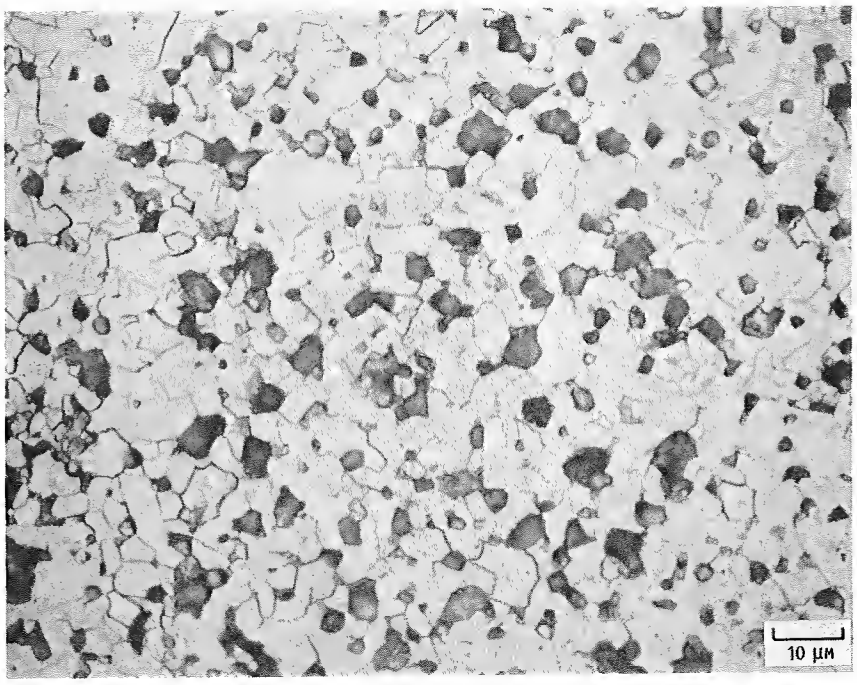

(A) AS-RECEIVED STATE.

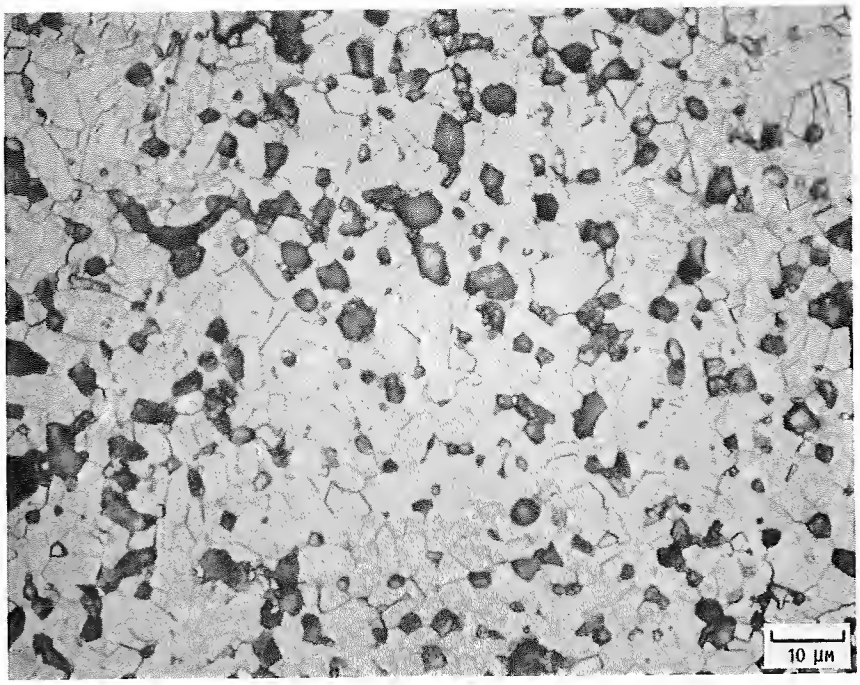

(B) AFTER TESTING AT 1400 ^{o}C. (1000X).

FIGURE 10. - ETCHED MICROSTRUCTURE OF TiB_2/SiC.

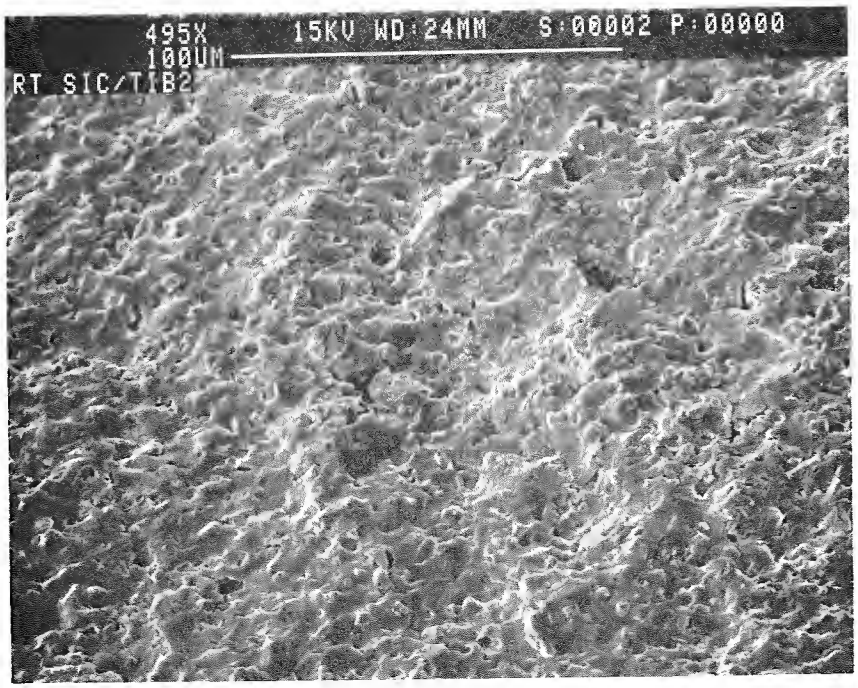

(A) 20 ^{o}C TESTS.

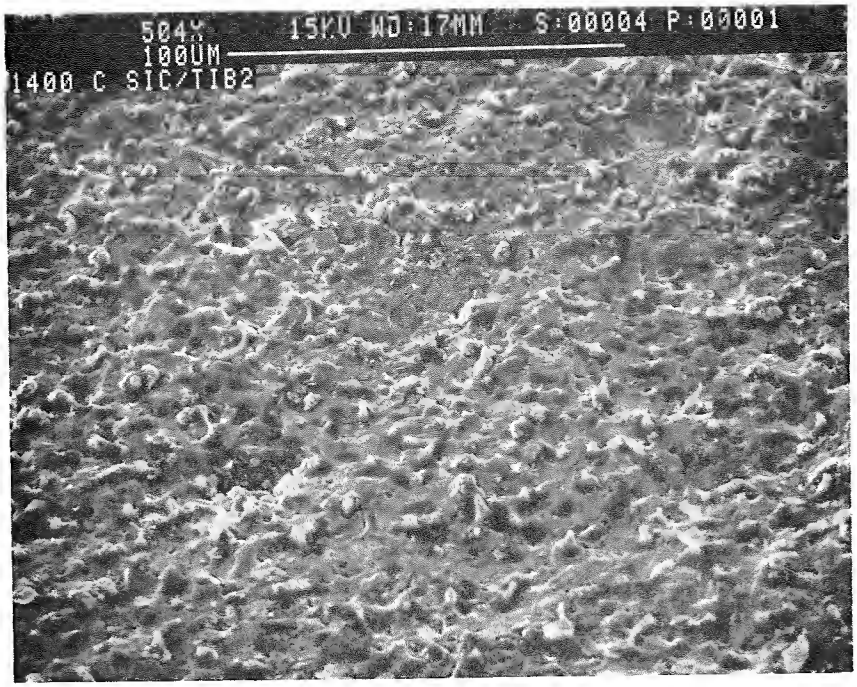

(B) 1400 ^{o}C TESTS.

FIGURE 11. - FRACTURE TOPOGRAPHY TiB_2/SiC.

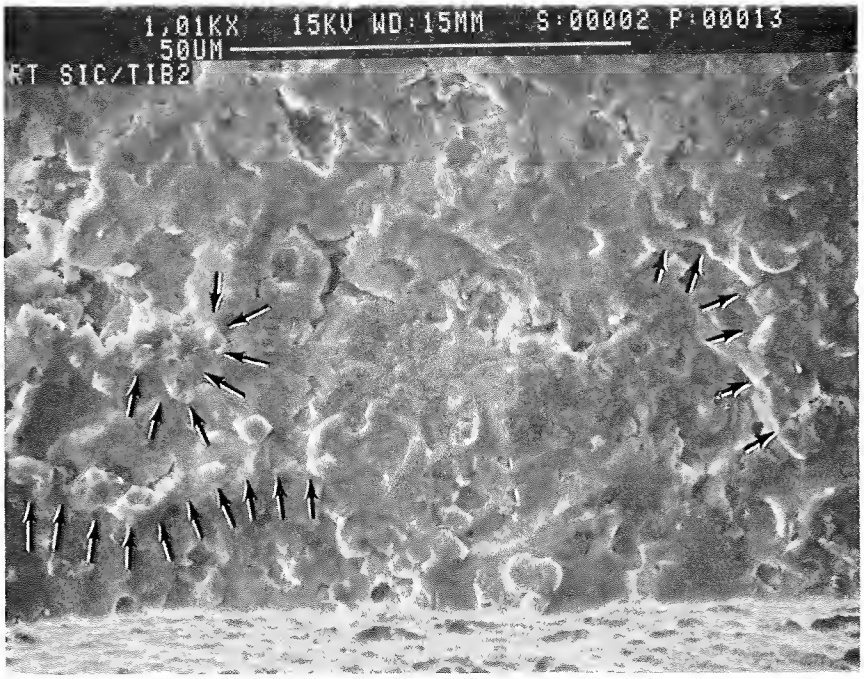

(A) SECONDARY ELECTRON MODE.

(B) BACKSCATTERED MODE.

FIGURE 12. - FRACTURE RIDGES.

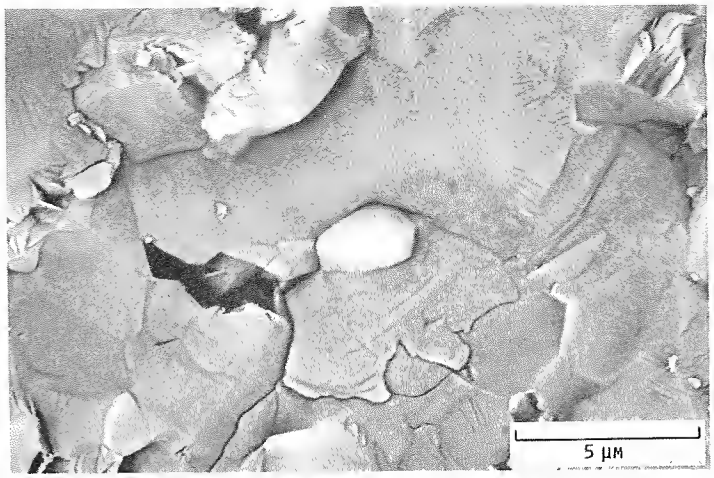

(A) 20 ^{o}C TESTS.

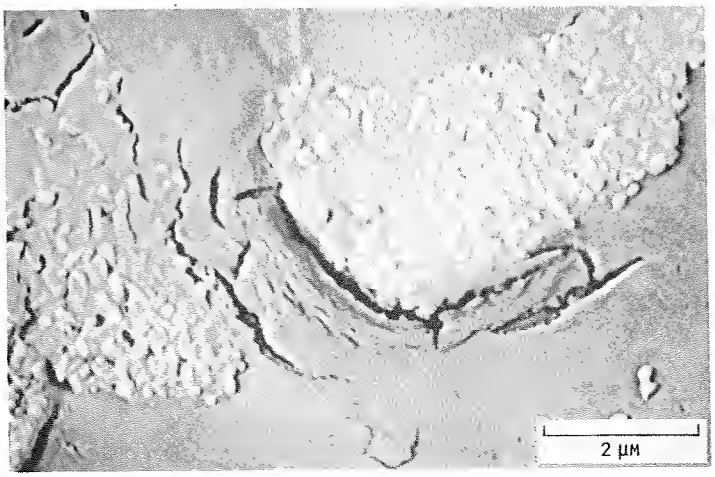

(B) 1400 ^{o}C TESTS.

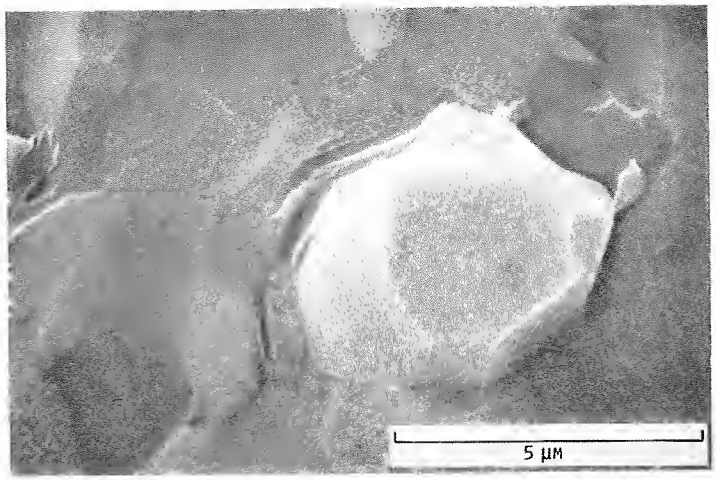

(C) 1400 ^{o}C TESTS.

FIGURE 13. - PARTICLE/MATRIX CRACKING AND SEPARATION.

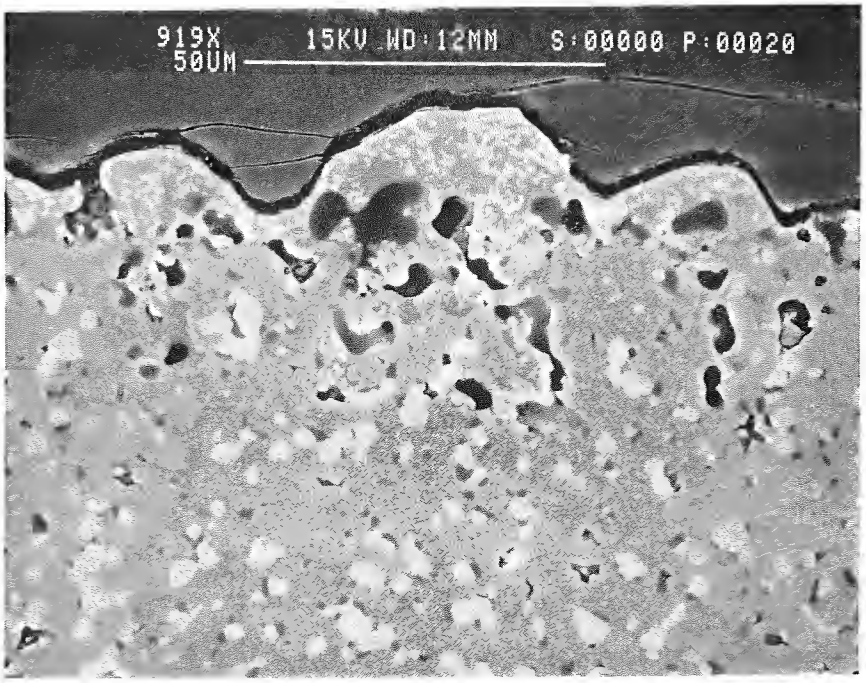

FIGURE 14. - SURFACE OXIDATION AND PITTING OF TiB_2/SiC EXPOSED TO 1400 ^{o}C TESTING.

NASA
National Aeronautics and Space Administration

Report Documentation Page

1. Report No.	2. Government Accession No.	3. Recipient's Catalog No.
NASA TM-100967		

4. Title and Subtitle
Fracture Resistance of a TiB_2 Particle/SiC Matrix Composite at Elevated Temperature

5. Report Date
June 1988

6. Performing Organization Code

7. Author(s)
Michael G. Jenkins, Jonathan A. Salem, and Srinivasa G. Seshadri

8. Performing Organization Report No.
E-3842-1

10. Work Unit No.
505-63-1B

9. Performing Organization Name and Address
National Aeronautics and Space Administration
Lewis Research Center
Cleveland, Ohio 44135-3191

11. Contract or Grant No.

13. Type of Report and Period Covered
Technical Memorandum

12. Sponsoring Agency Name and Address
National Aeronautics and Space Administration
Washington, D.C. 20546-0001

14. Sponsoring Agency Code

15. Supplementary Notes
Michael G. Jenkins, Institute of Industrial Science, University of Tokyo, Tokyo, Japan; currently an invited researcher at NASA Lewis Research Center. Jonathan A. Salem, NASA Lewis Research Center. Srinivasa G. Seshadri, Standard Oil Engineered Materials Company, P.O. Box 1054, Niagara Falls, New York 14302.

16. Abstract

The fracture resistance of a commercial TiB_2 particle/SiC matrix composite was evaluated at temperatures ranging from 20 to 1400 °C. A laser interferometric strain gauge (LISG) was used to continuously monitor the crack mouth opening displacement (CMOD) of the chevron-notched and straight-notched, three-point bend specimens used. Crack growth resistance curves (R-curves) were determined from the load versus displacement curves and displacement calibrations. Fracture toughness, work-of-fracture, and R-curve levels were found to decrease with increasing temperature. Microstructure, fracture surface, and oxidation coat were examined to explain the fracture behavior.

17. Key Words (Suggested by Author(s))	18. Distribution Statement
Fracture; Composite; Ceramic; SiC/TiB_2; Crack growth; High-temperature; Chevron-notch	Unclassified - Unlimited Subject Category 27

19. Security Classif. (of this report)	20. Security Classif. (of this page)	21. No of pages	22. Price*
Unclassified	Unclassified	18	A02

NASA FORM 1626 OCT 86

*For sale by the National Technical Information Service, Springfield, Virginia 22161